# Effect of channel thickness on noise in organic electrochemical transistors

*Anastasios G. Polyravas[1], Nathan Schaefer[2], Vincenzo F. Curto[1], Andrea Bonaccini Calia[2], Anton Guimera-Brunet[3,4], Jose A. Garrido[2,5] and George G. Malliaras[1,*]*

[1] Electrical Engineering Division, Department of Engineering, University of Cambridge, 9 JJ Thomson Ave, Cambridge CB3 0FA, United Kingdom
[2] Catalan Institute of Nanoscience and Nanotechnology (ICN2), CSIC, Barcelona Institute of Science and Technology, Campus UAB, 08193, Bellaterra, Barcelona, Spain
[3] Institut de Microelectronica de Barcelona, IMB-CNM (CSIC), 08193, Bellaterra, Barcelona, Spain
[4] Centro de Investigación Biomédica en Red en Bioingeniería, Biomateriales y Nanomedicina (CIBER-BBN), 28029, Madrid, Spain
[5] ICREA, Pg. Lluís Companys 23, 08010 Barcelona, Spain
* Corresponding author. Email: gm603@cam.ac.uk

## Abstract

Organic electrochemical transistors (OECTs) have been widely used as transducers in electrophysiology and other biosensing applications. Their identifying characteristic is a transconductance that increases with channel thickness, and this provides a facile mechanism to achieve high signal amplification. However, little is known about their noise behaviour. Here, we investigate noise and extract metrics for signal-to-noise ratio and limit of detection in OECTs with different channel thickness. These metrics are shown to improve as channel thickness increases, demonstrating that OECTs can be easily optimised to show not only high amplification, but also low noise.

Originally developed by White and colleagues[1], organic electrochemical transistors have been attracting a great deal of attention due to a combination of advantages that include simple structure and high performance[2]. Their mechanism of operation involves changes in the conductivity of a semiconductor film induced by ions injected/extracted from an adjacent electrolyte[3]. A gate electrode immersed in the electrolyte controls this process, and the resulting change in the doping state of the semiconductor is reflected in the drain current. The latter is induced by a voltage applied between source and drain electrodes that make contact to the semiconductor film. The simple structure of OECTs lends itself to fabrication by traditional photolithography[4] but also by low-cost printing techniques[5], onto a variety of substrates that include plastic[6], paper[7] and textile fibres[8]. OECTs have found many applications as transducers in applications[9,10], including electrophysiology[11–15], biosensing[16–19] and *in vitro* systems[20,21].

In the vast majority of these applications, OECTs are used as transducers that convert a voltage change at the gate $\partial V_g$ to a modulation in the drain current $\partial I_d$ [2]. This process is described by the transconductance $g_m=\partial I_d/\partial V_g$, which is directly linked to the ability of OECTs to amplify recorded signals[22]. As a result, a great deal of effort has focused on understanding how to improve transconductance by tuning device geometry[22,23], optimising materials design[24] and developing new device architectures[25]. OECTs made of PEDOT:PSS, a commercially available *p*-type semiconductor, show transconductance in the mS range, outperforming transistors from both traditional and emerging semiconductors[6]. Contrary to field-effect transistors, where changes in conductivity take place in a thin channel adjacent to the gate insulator, it is the conductivity of the entire semiconductor film that is modulated in OECTs. This means that the transistor channel in OECTs is defined by the dimensions of the semiconductor film between the source and drain contacts. As a result, the transconductance scales with channel thickness[23], and this has become an identifying characteristic of OECTs[26]. This means that one can reach arbitrarily high values of transconductance by simply increasing channel thickness, and OECs with $g_m$=1 S have been demonstrated[27].

Despite the interest in transconductance, little attention has been paid to understanding noise in OECTs. Stoop et al. were the first to investigate noise in OECTs[28]. They quantified parameters that relate to signal-to-noise ratio (SNR) and limit of detection (LOD) and showed that PEDOT:PSS OECTs exhibit comparable noise to graphene transistors and only slightly higher noise than transistors based on carbon nanotubes and silicon nanowires. Moreover, their results suggested that large area channels maximise SNR. In a previous paper, we investigated the impact of overlap between the semiconductor and the source and drain contacts and showed that it does not affect the noise characteristics of PEDOT:PSS OECTs[29]. Here, we investigate how noise in OECTs scales with channel thickness. Importantly, we show that metrics for SNR and LOD improve with channel thickness. We discuss the origin of this behaviour and provide guidelines for optimising the performance of OECT-based transducers.

**Figure 1a** illustrates the geometry of OECTs that were developed for this study. The source and drain electrodes were photolithographically patterned onto a glass substrate, resulting in a 50 x 50 $\mu m^2$ channel. A dispersion of PEDOT:PSS was spun at multiple cycles to create films with thickness of 140 ± 14, 315 ± 74 and 1330 ± 75 nm (N = 6 devices per thickness group). Each cycle consisted of a soft pre-bake (one minute at 110$^o$C) before the deposition of subsequent layers of PEDOT:PSS. A 2 μm thick layer of parylene C (PaC) was used to insulate the gold interconnects of each transistor, leaving only the channel area exposed to an aqueous electrolyte. A Ag/AgCl electrode was submerged into the electrolyte. An optical micrograph of the channel of an OECT is shown in Figure 1b.

Figure 1c shows the variation of transconductance with gate voltage for three typical OECTs with different channel thickness. The transconductance was measured by grounding the source terminal and applying a voltage of -0.5 V at the drain terminal and a voltage varying from -0.6 to 0.6 V at the gate terminal. The resistive loss at the Au interconnects was taken into account to calculate the true values of the drain ($V_d$) and gate ($V_g$) voltage. The transconductance was also corrected to account for the true value of $V_d$ (Table S1 in Supplementary Information). The bell-shaped $g_m$ curves in Fig. 1c are

typical for PEDOT:PSS OECTs[30]. The maximum transconductance for the OECT with the thickest channel was 22.8 mS, a value that is 10.5 times and 3.8 times higher compared to OECTs with thickness of ~140 nm and ~315 nm, respectively. These results are in good agreement with previous work, which showed that the transconductance of OECTs is proportional to the thickness of the channel[23]. A shift in the voltage in which the peak transconductance is reached was also observed, consistent with previous reports[22]. More information about the characterisation of the OECTs can be found in the Supplementary Information (Figures S1 and S2).

The increase in the transconductance of OECTs with channel thickness is known to be accompanied by a decrease in the cut-off frequency[23]. This is shown in Figure 1d, where the normalised transconductance $g_{m,norm}$ is plotted as a function of frequency f. For this measurement, the OECTs were biased by applying -0.5 V at the drain terminal and a series of sine waves with frequency between 1 Hz to 20 kHz and amplitude of 50 mV were applied at the gate terminal. A 7.2 times decrease (998 Hz compared to 138 Hz) in the cut-off frequency was observed when the channel thickness was varied from ~140 nm to ~1330 nm. The cut-off frequencies of the OECTs were consistent with an RC equivalent circuit model of the gate/electrolyte/channel circuit (Table S2 in Supplementary Information).

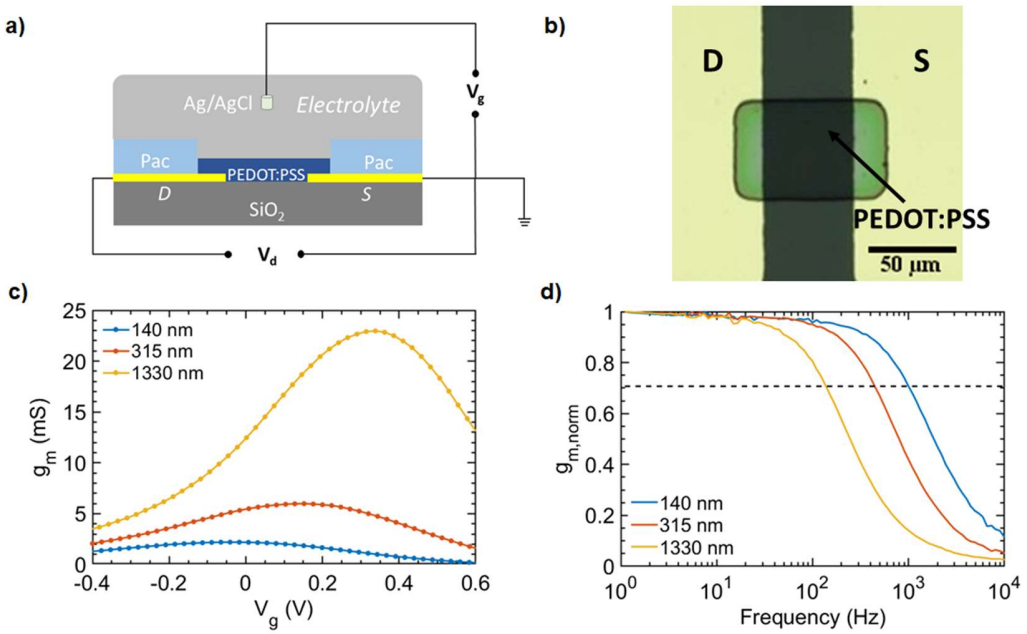


**Figure 1**. a) Schematic of the cross section of an OECT illustrating the biasing configuration. b) Optical micrograph of an OECT. c) Transconductance vs. gate voltage of OECTs with different thickness. Both $g_m$ and $V_g$ were corrected for resistive loss at interconnects. The lines are guides to the eye. d) Normalised transconductance vs. frequency with the dashed line corresponding to the cut-off frequency (-3dB).

The noise characteristics of the OECTs were examined next. The power spectral density of the drain current $S_{Id}$ was obtained by measuring the fluctuations of the drain current in the time domain and converting the data to the frequency domain (see device characterisation below). **Figure 2a** shows that the $S_{Id}$ of an OECT with ~130 nm channel thickness follows the 1/f law (plots for the OECTs made of thicker films can be found in Figure S3). This is a typical characteristic of flicker noise and was observed in frequencies lower than 100 Hz, in agreement with previous studies in thin film transistors[31,32], including OECTs[28,29]. As dedoping of the PEDOT:PSS film occurs at high gate voltages, thermal noise begins to flatten the $S_{Id}$ vs frequency curves. A similar trend was detected in the normalised power spectral density $S_{Id}/I_d^2$ (Figure S4), a figure-of-merit that is used to compare noise across different device architectures and bias conditions[33,34]. In Figure 2b, we used this normalisation to compare OECTs with channels of different thickness. $S_{Id}/I_d^2$

was evaluated at 10 Hz, the frequency of the alpha rhythm of the brain, which is widely used in electroencephalography. Each point in the graph represents the mean value measured from six OECTs with the same nominal channel thickness, with the error bars corresponding to the standard deviation. As seen in Figure 2b, the relative noise decreases with channel thickness, with the OECT with the ~1330 nm thick channel showing the lowest values. It should be noted that values of $V_g$ were corrected for resistive loss at interconnects.

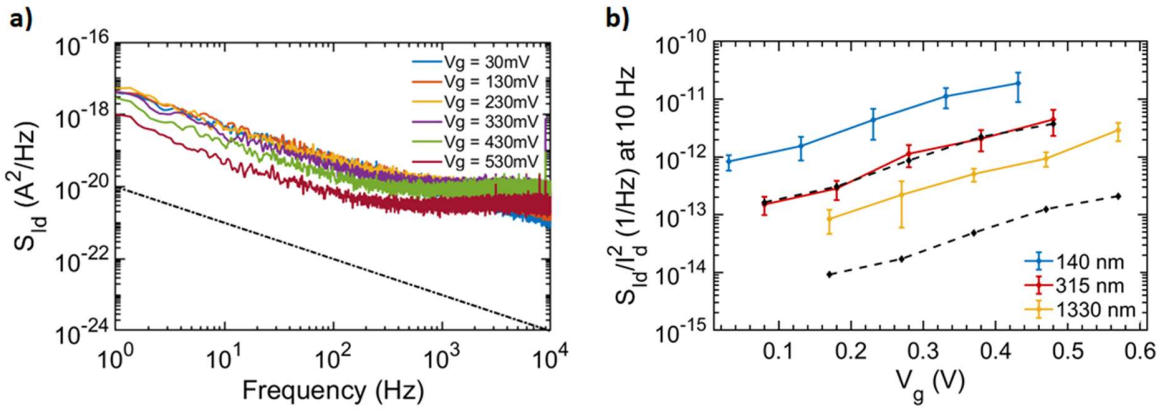


**Figure 2**. a) Power spectral density $S_{Id}$ vs. frequency for an OECT with ~130 nm channel thickness. The dashed line has a slope of 1/f, indicating that flicker noise is the dominant contributor to noise at low frequencies. b) Normalised power spectral density $S_{Id}/I_d^2$ vs. gate voltage for OECTs with different thickness. Each point corresponds to the mean value (N = 6 transistors), with the error bars indicating the standard deviation. The solid lines are guides to the eye. $V_g$ was corrected for resistive loss at interconnects. The dashed lines correspond to the scaling predicted by the charge noise model.

The noise behaviour of electrolyte-gated transistors[31,35,36], including OECTs[28], is usually discussed in the context of the charge noise model. This model assumes that flicker noise originates from fluctuations in the number of charge carriers in the channel of the transistor[37]. It postulates that the normalised power spectral density $S_{Id}/I_d^2$ scales with the ratio $g_m^2/I_d^2$, a scaling that seems to hold in our OECTs (Figure S6 in the Supplementary Information). Moreover, $S_{Id}/I_d^2$ is inversely proportional to the square of the gate capacitance[28,33]. As the capacitance of OECTs increases with channel thickness, $S_{Id}/I_d^2$

is expected to scale as $1/d^2$. The dashed lines in Fig. 2B reflect the expected scaling for the OECTs with channel thickness of ~315 nm and ~1330 nm using the relative noise for the transistor with the thinnest channel as a starting point. While good agreement is obtained for the transistor with the ~315 nm thick channel, the relative noise predicted for the transistor with the ~1330 nm thick channel is about 10 times lower that the measured values. We discuss this discrepancy below.

In addition to relative noise, parameters that relate to SNR and LOD are used to characterise and compare transducers. One such parameter is the square root of the gate referred voltage noise $S_{Vg}^{1/2}$, which is obtained by dividing $S_{Id}^{1/2}$ by the transconductance. As such, it is used as a way to estimate SNR when the transistor is used as a voltage sensor (the lower $S_{Vg}^{1/2}$, the higher the SNR)[28,32]. **Figure 3a** shows that $S_{Vg}^{1/2}$ increases with gate voltage and, more importantly, decreases with thickness. The dashed lines reflect the expected scaling for the OECTs with channel thickness of ~315 nm and ~1330 nm using the gate referred voltage noise for the transistor with the thinnest channel as a starting point. As with the relative noise, the model agrees with the data obtained from the OECT with the ~315 nm thick channel but predicts lower values for the OECT with the ~1330 nm thick channel. It should be noted that the value of 50 $nV/Hz^{1/2}$ obtained in the OECT with the thickest channel compares favourably with values reported in other thin film transistor technologies[31,36,38].

Another important metric for transistors when used as voltage transducers is $V_{rms}$. This parameter is obtained by dividing the square root of the integral of $S_{Id}$ over a frequency window of interest by the transconductance[35,39]. As such, it quantifies the LOD, or the minimum voltage that can be detected by the transistor. Figure 3b shows the calculated $V_{rms}$ of eighteen different OECTs as a function of transconductance. $V_{rms}$ was calculated in the range of 1-100 Hz and with 0 V applied at the gate terminal ($V_{rms}$ calculated at $V_g$ corresponding to maximum transconductance, shown in Fig. S5, shows a similar trend). $V_{rms}$ decreases with transconductance (hence channel thickness), reaching its lowest value of ~0.4 μV for the OECTs with the thickest channels. $V_{rms}$ values in different frequency bandwidths are shown in Table S3 in Supplementary Information. Based on these values, OECTs compare favourably to reported values of transistors[39] and

electrodes[40] from other materials. It should be noted that the thermal noise added by the Au interconnects is 12.28 nV (1-100 Hz range), hence negligible.

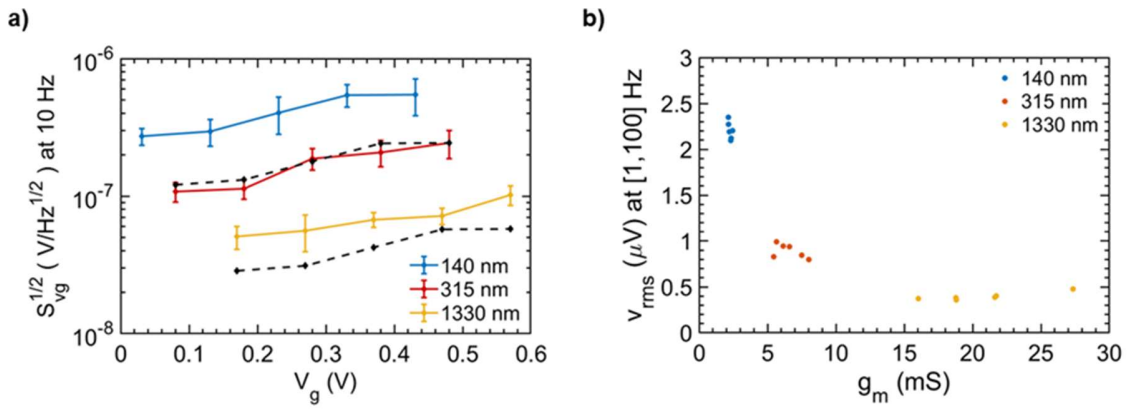


**Figure 3**. a) Root square gate voltage noise vs. gate voltage for OECTs with different thickness. Each point corresponds to the mean value (N = 6 transistors), with the error bars indicating the standard deviation. The solid lines are guides to the eye. $V_g$ was corrected for resistive loss at interconnects. The dashed lines correspond to the scaling predicted by the charge noise model. b) Root mean square of the voltage fluctuations in the 1 Hz to 100 Hz band vs. transconductance. $V_{rms}$ values were calculated for 0 V applied at the gate terminal.

The volumetric capacitance of organic materials such as PEDOT:PSS is leveraged in several applications in bioelectronics[41]. OECTs utilise this property to achieve high transconductance, which translates to high signal amplification[6]. This comes at the expense of cut-off frequency, as volumetric charging is a slow process. Still, OECTs have found applications in biosensing and electrophysiology, where signals rage from quasi-DC up to several kHz[42]. Tuning device performance is achieved chiefly by selecting the appropriate channel thickness that maximizes transconductance while maintaining an acceptable cut-off frequency[23]. The results obtained here for transconductance and cut-off frequency of the OECTs with channels of different thickness (Fig. 1c-d) confirm this trade-off and are in quantitative agreement with the predictions of the Bernards model. With respect to noise, we found that the relative noise in OECTs decreases in OECTs with thicker channels. This means that a large channel thickness is not only desirable

because it increases transconductance but also because it decreases SNR and LOD. The main limitation in performance is still the cut-off frequency. A recent OECT design has shown that this limit can be overcome to a significant degree[15].

We found that the decrease in noise measured when the channel thickness increased from 140 nm 315 nm was consistent with the prediction of the charge noise model that $S_{Id}/I_d^2$ is inversely proportional to the square of the gate capacitance. However, when the channel thickness increased to 1330 nm, the model underestimated the measured values of noise. A more sophisticated model that considers fluctuations in both carrier number and carrier mobility was developed for field-effect transistors[33,43]. This model introduces an additional factor in $S_{Id}/I_d^2$ that is proportional to the gate capacitance and hence predicts a more moderate decrease of relative noise with channel thickness. Unfortunately, this additional factor does not appear when the model is derived for OECTs (see Supplementary Information), and therefore the model cannot account for the deviation observed in the OECT with the thickest channel. As it currently stands, we do not understand this deviation.

In conclusion, we investigated the impact of channel thickness on the noise characteristics of PEDOT:PSS OECTs. We found that normalised noise decreases with channel thickness. When the channel thickness increased from 140 nm 315 nm, the decrease in noise was consistent with the prediction of the charge noise model. However, when the channel thickness increased to 1330 nm, the charge noise model underestimated the measured values. Similar trends are observed in metrics for the signal-to-noise ratio and limit of detection, which revealed that OECTs compare favourably to other transistor technologies, including graphene transistors and electrodes. This work shows that OECT-based transducers should be designed for the maximum possible thickness, as determined by the cut-off frequency requirements of the application.

# Supplementary Material

The supplementary material contains information about the fabrication and the characterisation of OECTs, as well as the noise model developed for this study. It also contains some extra figures (S1-S6) and tables (S1-S2) to provide with some better understanding of this work and support the data presented in this paper.

# Acknowledgements

This work was funded by the European Union's Horizon 2020 research and innovation programme under grant agreement no. 732032 (BrainCom) the King Abdullah University of Science and Technology (KAUST) Office of sponsored Research (OSR) under award No. OSR-2016-CRG5-3003. Thanks are due to Elise Jenkins for help with the model.

# Data availability

The data that support the findings of this study are available from the corresponding author upon reasonable request.

# References

1. White, H. S., Kittlesen, G. P. & Wrighton, M. S. Chemical derivatization of an array of three gold microelectrodes with polypyrrole: fabrication of a molecule-based transistor. *J. Am. Chem. Soc.* **106**, 5375–5377 (1984).
2. Rivnay, J., Inal, S., Salleo, A., Owens, R. M., Berggren, M. & Malliaras, G. G. Organic electrochemical transistors. *Nature Reviews Materials* **3**, 17086 (2018).
3. Bernards, D. A. & Malliaras, G. G. Steady-State and Transient Behavior of Organic Electrochemical Transistors. *Adv. Funct. Mater.* **17**, 3538–3544 (2007).
4. Sessolo, M., Khodagholy, D., Rivnay, J., Maddalena, F., Gleyzes, M., Steidl, E., Buisson, B. & Malliaras, G. G. Easy-to-Fabricate Conducting Polymer Microelectrode Arrays. *Adv. Mater.* **25**, 2135–2139 (2013).
5. Andersson Ersman, P., Lassnig, R., Strandberg, J., Tu, D., Keshmiri, V., Forchheimer, R., Fabiano, S., Gustafsson, G. & Berggren, M. All-printed large-scale integrated circuits based on organic electrochemical transistors. *Nature Communications* **10**, 1–9 (2019).
6. Khodagholy, D., Rivnay, J., Sessolo, M., Gurfinkel, M., Leleux, P., Jimison, L. H., Stavrinidou, E., Herve, T., Sanaur, S., Owens, R. M. *et al.* High transconductance organic electrochemical transistors. *Nature Communications* **4**, 2133 (2013).

7. Nilsson, D., Kugler, T., Svensson, P.-O. & Berggren, M. An all-organic sensor–transistor based on a novel electrochemical transducer concept printed electrochemical sensors on paper. *Sensors and Actuators B: Chemical* **86**, 193–197 (2002).
8. Hamedi, M., Herlogsson, L., Crispin, X., Marcilla, R., Berggren, M. & Inganäs, O. Fiber-Embedded Electrolyte-Gated Field-Effect Transistors for e-Textiles. *Advanced Materials* **21**, 573–577 (2009).
9. Strakosas, X., Bongo, M. & Owens, R. M. The organic electrochemical transistor for biological applications. *Journal of Applied Polymer Science* **132**, (2015).
10. Bai, L., Elósegui, C. G., Li, W., Yu, P., Fei, J. & Mao, L. Biological Applications of Organic Electrochemical Transistors: Electrochemical Biosensors and Electrophysiology Recording. *Front. Chem.* **7**, (2019).
11. Khodagholy, D., Doublet, T., Quilichini, P., Gurfinkel, M., Leleux, P., Ghestem, A., Ismailova, E., Herve, T., Sanaur, S., Bernard, C. *et al. In vivo* recordings of brain activity using organic transistors. *Nature Communications* **4**, 1575 (2013).
12. Campana, A., Cramer, T., Simon, D. T., Berggren, M. & Biscarini, F. Electrocardiographic Recording with Conformable Organic Electrochemical Transistor Fabricated on Resorbable Bioscaffold. *Advanced Materials* **26**, 3874–3878 (2014).
13. Williamson, A., Ferro, M., Leleux, P., Ismailova, E., Kaszas, A., Doublet, T., Quilichini, P., Rivnay, J., Rozsa, B., Katona, G. *et al.* Localized Neuron Stimulation with Organic Electrochemical Transistors on Delaminating Depth Probes. *Adv. Mater.* **27**, 4405–4410 (2015).
14. Leleux, P., Rivnay, J., Lonjaret, T., Badier, J.-M., Bénar, C., Hervé, T., Chauvel, P. & Malliaras, G. G. Organic Electrochemical Transistors for Clinical Applications. *Advanced Healthcare Materials* **4**, 142–147 (2015).
15. Cea, C., Spyropoulos, G. D., Jastrzebska-Perfect, P., Ferrero, J. J., Gelinas, J. N. & Khodagholy, D. Enhancement-mode ion-based transistor as a comprehensive interface and real-time processing unit for in vivo electrophysiology. *Nature Materials* 1–8 (2020) doi:10.1038/s41563-020-0638-3.
16. Zhang, M., Liao, C., Mak, C. H., You, P., Mak, C. L. & Yan, F. Highly sensitive glucose sensors based on enzyme-modified whole-graphene solution-gated transistors. *Sci Rep* **5**, (2015).
17. Pappa, A.-M., Curto, V. F., Braendlein, M., Strakosas, X., Donahue, M. J., Fiocchi, M., Malliaras, G. G. & Owens, R. M. Organic Transistor Arrays Integrated with Finger-Powered Microfluidics for Multianalyte Saliva Testing. *Advanced Healthcare Materials* **5**, 2295–2302 (2016).
18. Braendlein, M., Pappa, A.-M., Ferro, M., Lopresti, A., Acquaviva, C., Mamessier, E., Malliaras, G. G. & Owens, R. M. Lactate Detection in Tumor Cell Cultures Using Organic Transistor Circuits. *Advanced Materials* **29**, 1605744 (2017).
19. Curto, V. F., Marchiori, B., Hama, A., Pappa, A., Ferro, M. P., Braendlein, M., Rivnay, J., Fiocchi, M., Malliaras, G. G., Ramuz, M. *et al.* Organic transistor platform with integrated microfluidics for in-line multi-parametric *in vitro* cell monitoring. *Microsystems & Nanoengineering* **3**, 17028 (2017).
20. Pitsalidis, C., Pappa, A., Porel, M., Artim, C. M., Faria, G. C., Duong, D. D., Alabi, C. A., Daniel, S., Salleo, A., Owens, R. M. Biomimetic Electronic Devices for Measuring Bacterial Membrane Disruption. *Advanced Materials* **30**, 1803130 (2018).
21. Pitsalidis, C., Ferro, M. P., Iandolo, D., Tzounis, L., Inal, S. & Owens, R. M. Transistor in a tube: A route to three-dimensional bioelectronics. *Science Advances* **4**, eaat4253 (2018).
22. Rivnay, J., Leleux, P., Sessolo, M., Khodagholy, D., Hervé, T., Fiocchi, M. & Malliaras, G. G. Organic electrochemical transistors with maximum transconductance at zero gate bias. *Adv. Mater. Weinheim* **25**, 7010–7014 (2013).

23. Rivnay, J., Leleux, P., Ferro, M., Sessolo, M., Williamson, A., Koutsouras, D. A., Khodagholy, D., Ramuz, M., Strakosas, X., Owens, R. M. *et al.* High-performance transistors for bioelectronics through tuning of channel thickness. *Science Advances* **1**, e1400251 (2015).
24. Giovannitti, A., Sbircea, D., Inal, S., Nielsen, C. B., Bandiello, E., Hanifi, D. A., Sessolo, M., Malliaras, G. G., McCullocj, I., Rivnay, J. Controlling the mode of operation of organic transistors through side-chain engineering. *PNAS* **113**, 12017–12022 (2016).
25. Spyropoulos, G. D., Gelinas, J. N. & Khodagholy, D. Internal ion-gated organic electrochemical transistor: A building block for integrated bioelectronics. *Science Advances* **5**, eaau7378 (2019).
26. Inal, S., Malliaras, G. G. & Rivnay, J. Benchmarking organic mixed conductors for transistors. *Nature Communications* **8**, 1767 (2017).
27. Malti, A., Edberg, J., Granberg, H., Khan, Z. U., Andreasen, J. W., Liu, X., Zhao, D., Zhang, H., Yao, Y., Brill, J. W. *et al.* An Organic Mixed Ion-Electron Conductor for Power Electronics. *Adv Sci (Weinh)* **3**, 1500305 (2016).
28. Stoop, R. L., Thodkar, K., Sessolo, M., Bolink, H. J., Schönenberger, C. & Calame, M. Charge Noise in Organic Electrochemical Transistors. *Phys. Rev. Applied* **7**, 014009 (2017).
29. Polyravas, A. G., Curto, V. F., Schaefer, N., Calia, A. B., Guimera-Brunet, A., Garrido, J. A. & Malliaras, G. G. Impact of contact overlap on transconductance and noise in organic electrochemical transistors. *Flex. Print. Electron.* **4**, 044003 (2019).
30. Friedlein, J. T., Rivnay, J., Dunlap, D. H., McCulloch, I., Shaheen, S. E., McLeod, R. R. & Malliaras, G. G. Influence of disorder on transfer characteristics of organic electrochemical transistors. *Appl. Phys. Lett.* **111**, 023301 (2017).
31. Heller, I., Chatoor, S., Männik, J., Zevenbergen, M. A. G., Oostinga, J. B., Morpurgo, A. F., Dekker, C. & Lemay, S. G. Charge Noise in Graphene Transistors. *Nano Lett.* **10**, 1563–1567 (2010).
32. Clément, N., Nishiguchi, K., Dufreche, J. F., Guerin, D., Fujiwara, A. & Vuillaume, D. A silicon nanowire ion-sensitive field-effect transistor with elementary charge sensitivity. *Appl. Phys. Lett.* **98**, 014104 (2011).
33. Liu, Y., He, H., Chen, R., En, Y.-F., Li, B. & Chen, Y.-Q. Analysis and Simulation of Low-Frequency Noise in Indium-Zinc-Oxide Thin-Film Transistors. *IEEE Journal of the Electron Devices Society* **6**, 271–279 (2018).
34. Choi, H.-S., Jeon, S., Kim, H., Shin, J., Kim, C. & Chung, U.-I. The impact of active layer thickness on low-frequency noise characteristics in InZnO thin-film transistors with high mobility. *Appl. Phys. Lett.* **100**, 173501 (2012).
35. Sharf, T., Kevek, J. W., DeBorde, T., Wardini, J. L. & Minot, E. D. Origins of Charge Noise in Carbon Nanotube Field-Effect Transistor Biosensors. *Nano Lett.* **12**, 6380–6384 (2012).
36. Bedner, K., Guzenko, V. A., Tarasov, A., Wipf, M., Stoop, R. L., Rigante, S., Brunner, J., Fu, W., David, C., Calame, M. *et al.* Investigation of the dominant 1/f noise source in silicon nanowire sensors. *Sensors and Actuators B: Chemical* **191**, 270–275 (2014).
37. Tersoff, J. Low-Frequency Noise in Nanoscale Ballistic Transistors. *Nano Lett.* **7**, 194–198 (2007).
38. Männik, J., Heller, I., Janssens, A. M., Lemay, S. G. & Dekker, C. Charge Noise in Liquid-Gated Single-Wall Carbon Nanotube Transistors. *Nano Lett.* **8**, 685–688 (2008).
39. Hébert, C., Masvidal-Codina, E., Suarez-Perez, A., Calia, A. B., Piret, G., Garcia-Cortadella, R., Illa, X., Garcia, E. D. C., Sanchez, J. M. D. la C., Casals, D. V. *et al.* Flexible Graphene Solution-Gated Field-Effect Transistors: Efficient Transducers for Micro-Electrocorticography. *Advanced Functional Materials* **28**, 1703976 (2018).
40. Kuzum, D., Takano, H., Shim, E., Reed, J. C., Juul, H., Richardson, A. G., Vries, J., Bink, H., Dichter, M. A., Lucas, T. H. *et al.* Transparent and flexible low noise graphene electrodes for simultaneous electrophysiology and neuroimaging. *Nature Communications* **5**, 1–10 (2014).

41. Proctor, C. M., Rivnay, J. & Malliaras, G. G. Understanding volumetric capacitance in conducting polymers. *Journal of Polymer Science Part B: Polymer Physics* **54**, 1433–1436 (2016).
42. Buzsaki, G. *Rhythms of the Brain*. (Oxford University Press, U.S.A., 2011).
43. Ghibaudo, G., Roux, O., Nguyen-Duc, C., Balestra, F. & Brini, J. Improved Analysis of Low Frequency Noise in Field-Effect MOS Transistors. *physica status solidi (a)* **124**, 571–581 (1991).